New Journal of Physics
The open access journal at the forefront of physics

Deutsche Physikalische Gesellschaft DPG IOP Institute of Physics

PAPER • OPEN ACCESS

Hyper-Raman lines emission concomitant with high-order harmonic generation

To cite this article: Etienne Bloch *et al* 2019 *New J. Phys.* **21** 073006

New Journal of Physics
The open access journal at the forefront of physics

Deutsche Physikalische Gesellschaft DPG
IOP Institute of Physics

Published in partnership with: Deutsche Physikalische Gesellschaft and the Institute of Physics

OPEN ACCESS

RECEIVED
10 September 2018

REVISED
27 May 2019

ACCEPTED FOR PUBLICATION
11 June 2019

PUBLISHED
1 July 2019

PAPER

Hyper-Raman lines emission concomitant with high-order harmonic generation

Etienne Bloch[1], **Samuel Beaulieu**[1,2,3], **Dominique Descamps**[1], **Stéphane Petit**[1], **François Légaré**[2], **Alexander Magunov**[4], **Yann Mairesse**[1] **and Vasily Strelkov**[4,5]

[1] Université de Bordeaux—CNRS—CEA, CELIA, UMR5107, F-33405 Talence, France
[2] ALLS, Institut National de la Recherche Scientifique, Centre EMT, J3X1S2, Varennes, Quebec, Canada
[3] Fritz Haber Institut of the Max Planck Society, Faradayweg 4-6, D-14195 Berlin, Germany
[4] Prokhorov General Physics Institute of the Russian Academy of Sciences, Theoretical Department, 38, Vavilova St., Moscow 119991, Russia
[5] Moscow Institute of Physics and Technology (State University), 141700 Dolgoprudny, Moscow Region, Russia

E-mail: etienne.bloch@u-bordeaux.fr

Keywords: hyper-Raman lines, high-order harmonic generation, ultrafast spectroscopy, nonlinear optics, strong field physics, XUV free induction decay

Abstract

Hyper-Raman lines (HRL) resulting from strong-field light–matter interaction have been predicted theoretically in the 1990s but never identified in high-order harmonic generation experiments. Here, we use a combination of 800 and 400 nm laser pulses to control independently the two processes required for the hyper-Raman emission: creation of a coherence between two electronic states and laser-dressing of these states. As a result we observe simultaneously high-order harmonics, XUV free induction decay and HRL. We investigate experimentally and numerically the properties of this novel emission source. It can be of high interest, amongst others, for high-resolution spatio-temporal spectroscopy of excited electronic states in the same fashion high-order harmonics generation provides it for ground state.

1. Introduction

The interaction of strong laser fields with atoms results in the emission of coherent extreme ultraviolet (XUV) radiation as high-order harmonics of the fundamental frequency [1, 2]. This process, which is at the foundation of attosecond spectroscopy [3], has been successfully modeled for several decades within the framework of the Strong-Field Approximation [4], which provides an excellent description of the main features of the XUV emission. One of the core assumptions of the SFA is to neglect the influence of bound excited states in the high-harmonic generation. However, as experiments get more sophisticated, coherent XUV emission processes involving these states are being discovered and investigated: XUV free-induction decay, either excited by single-photon [5, 6] or multiphoton absorption [7], high-order harmonic generation (HHG) from excited Rydberg states [8] or from frustrated tunnel ionization [9]. The XUV emission constitutes a spectroscopic signature of the strong-field dynamics involving the bound excited states, and could thus be used to resolve their dynamics. The perspective of applying these strong-field spectroscopies of bound dynamics to more complex cases, such as molecules or solid targets, is very appealing.

In the early days of HHG, many calculations of the emission spectrum of atoms in strong laser fields predicted not only odd harmonics of the laser frequency, but also additional spectral features resulting from multiphoton absorption from excited states [10–17]. Indeed, if coherences are created between the ground state and excited states beside the HHG process, the wavepacket can be driven by the laser field and recombine coherently to the ground state, emitting photons at new frequencies. These spectral lines, located somewhere in between the usual high-order harmonics, are called hyper-Raman lines (HRL). If the system is in a coherent superposition of states (say states of energies E_1 and E_2), driven by a single color field of frequency ω_0, the

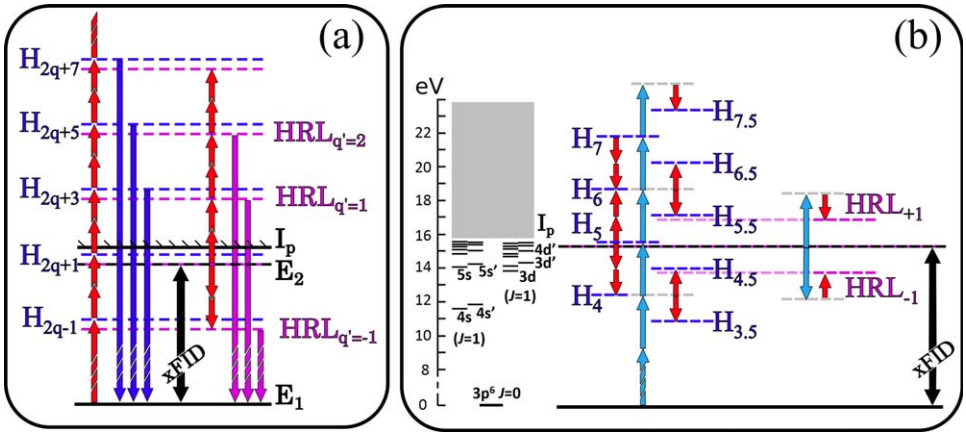

Figure 1. (a) Schematic of the simultaneous generation of high-order harmonics and hyper-Raman lines in a single-color strong-field driven atom. The driving laser photons are represented as red arrows, the HHG emission is represented as blue arrows and the HRL emission is represented as purple arrows. The double-sided black arrow represents the fact that the state of energy E_1 and E_2 are in coherent superposition, leading to xFID emission at $\Omega_{\mathrm{xFID}} = (E_2 - E_1)/\hbar$. (b) Left: energy diagram of argon. Right : schematic of the multiphoton processes experimentally detected in the two-color configuration presented. Light blue arrows represent the 400 nm photons and red arrows the 800 nm photons. Arrows corresponding to the final emission have been omitted for clarity. Harmonics orders are denoted according to the 400 nm energy.

frequencies of HRL of q'th order $\Omega_{q'}^{\mathrm{HRL}}$ are given by:

$$\Omega_{q'}^{\mathrm{HRL}} = \frac{(E_2 - E_1)}{\hbar} \pm 2q'\omega_0. \tag{1}$$

The HRL are thus interpreted as originating from a high-order Raman process, where many photons are absorbed from a state of energy E_2, followed by the emission of a single higher energy photon to decay to the state of energy E_1. For this emission to be coherent, the states of energy E_1 and E_2 must be in coherent superposition prior to the high-order Raman process. A scheme of the simultaneous generation of high-order harmonics and HRL is shown in figure 1(a). The creation of a coherence between the ground state and an excited state can also lead to emission features from the Free-Induction Decay process in the XUV range (xFID) [5, 7].

There is a number of theoretical and numerical papers where frequency components given by equation (1) are denoted as HRL [10–17]. Note, however, that in the spectroscopic community the term hyper-Raman scattering is used to describe components with frequencies $\Omega_q^{\mathrm{HRL}} = q\omega_0 - (E_2 - E_1)/\hbar$, see, for instance [18, 19]. In this process the initial state is the ground sate and the final one is the excited state, while in the process corresponding to equation (1) it is the other way around. In this paper we study the generation of the frequency components given by equation (1).

HRL have often been observed in simulations, while they have never been clearly identified experimentally. Emission involving dressed autoionizing states has recently been observed in HHG from laser-ablated tin plumes [20] but it has been interpreted a very different way using a four-step model based on the usual strong-field HHG three-step model with an extra step of wavepacket recombination. This puzzling discrepancy was interpreted as the result of the strict conditions required to observe HRL. First, one needs to be in a regime where the coherent superposition of states triggered by multiphoton resonant transitions is efficient [10]. Second, the AC-Stark-shifts induce strong variations of the frequency of the HRL with laser intensity. The HRL are thus strong and well-defined when calculating the single-atom response, with a temporally flat-top pulse. However the temporal and spatial variations of the laser intensity smears them out in macroscopic calculations and in experiments, where they most likely appear as a weak continuous background between the harmonic peaks. This effect of the Stark shift is expected to be even more critical at high laser intensity, in the regime where HHG is optimized. Here, we avoid such effects by working with rather weak laser fields, and by decoupling the excitation of electronic states and the generation of HHG and HRL using two laser pulses with different colors (400 and 800 nm, see figure 1(b)). This enables us to reveal unambiguously the signatures of hyper-Raman emission.

In the first part of the manuscript, we introduce the apparatus used in the experiment. In the second part we expose two theoretical models to understand the physical process. In the third part, we present the results and in the last part we discuss them and conclude.

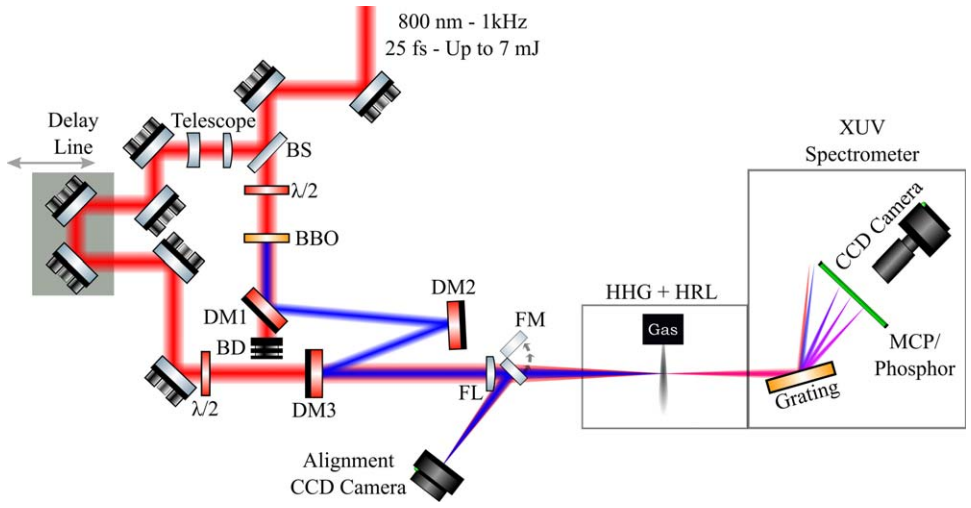

Figure 2. Sketch of the setup used for the experiment (see Experimental Set Up section for details). BS: beamsplitter, $\lambda/2$: half waveplate, DM: dichroic mirror, BD: beam dump, FL: focusing lens, FM: folding mirror.

2. Experimental set up

The experimental setup, sketched on figure 2, is based on the 800 nm Ti:Sa Aurore laser system at CELIA delivering 7 mJ–25 fs pulses at 1 kHz repetition rate. The beam was split in a Mach–Zender interferometer into a high-energy arm (90%) and a low-energy arm (10%). The former was frequency-doubled to 400 nm into a 200 μm thick BBO crystal. The latter was delayed by a pair of mirrors mounted on a translation stage and its intensity was controlled using a half waveplate combined with a polarizer. The cross correlation between the 400 and the 800 nm pulse is estimated to be $\sim$115 fs. The two beams were recombined using a dichroic mirror and focused by a $f = 1.5$ m lens into a 250 μm thick effusive gas jet of argon with linear, parallel polarizations. The thin nature of the gas jet ensures that processes involving the generation and reabsorption of XUV, as studied in two-jet experiments [6], are negligible. The XUV emission along the laser propagation axis was monitored by a flat-field XUV spectrometer made of a 1200 grooves mm^{-1} cylindrical grating and a stack of two microchannel plates (MCP) coupled to a phosphor screen. A CCD camera recorded the spatio-spectrally resolved signal from the phosphor screen fluorescence.

3. Theory

3.1. Numerical time-dependent Schrödinger equation (TDSE) solution

The interaction of the atom with the laser field is simulated solving numerically the 3D TDSE in the single-active electron approximation. We use the model potential for argon suggested in [21] and the numerical approach is described in [22]. The used model potential reproduces correctly the ground state energy and the energies of the two lowest excited states are close to the corresponding energies in the argon atom. The energies of the Rydberg states are also correctly reproduced. However, the ground state in this model potential is s-state, opposite to the p-state in argon. So, in real argon atom both transitions from s- and d-states to the ground state lead to emission of light, while in the numerical TDSE solution only transitions from the p-states are involved. Note that one can overcome this drawback using soft-core potential [23]. However, the latter modifies energies of the s-states and might add some 'artificial' channels in the multiphoton resonance picture. To escape this we use the model potential from [21].

3.2. Two-level model for transition to the Rydberg state

Another theoretical model which we have used in this study is the two-level system in the laser field. We solve numerically Bloch equations (see, for instance [24]). As we describe the resonances with the Rydberg states, we modify the approach used to study the HHG by the two-level system in the laser field [13, 16, 25]. This modification takes into account the fact that the transitions from the ground to the Rydberg states has rather low dipole matrix elements, but the Rydberg states' Stark-shift in the laser field is high. It was shown in [13, 25] that the Schrödinger equation in the two-level approximation can be written as the equation of an oscillator with the time-dependent frequency (i.e. as a parametric oscillator) driven by an external force (see equation (9) in [25]). This frequency is the nonlinear term leading to the harmonic generation and it is written as

$$\Omega = \omega_{10} + \Delta\Omega, \tag{2}$$

where ω_{10} is the unperturbed transition frequency, $\Delta\Omega$ is the Bloch–Siegert shift [24, 26] (atomic units are used throughout this section)

$$\Delta\Omega = 2V(t)^2/\omega_{10} \tag{3}$$

with $V(t) = dE(t)$ that describes an interaction of the system with the laser field $E(t)$, d is the dipole matrix element of the transition.

Here we introduce the effective dipole moment $d_{\rm eff}$ which is chosen so that $V_{\rm eff}(t) = d_{\rm eff}E(t)$ leads to

$$\Delta\Omega = \Delta\Omega_{\rm Stark}, \tag{4}$$

where $\Delta\Omega_{\rm Stark}$ is the change of the transition frequency due to the time-dependent Stark shift in the driving field. It is possible to satisfy equation (4) because both the Stark shift and the Bloch–Siegert shift are proportional to the laser intensity. The Stark shift of a Rydberg state under our conditions is close to the kinetic energy of the free electron oscillating in the laser field, and the Stark shift of the ground state can be neglected. So,

$$\Delta\Omega_{\rm Stark} = aE^2(t)/(2\omega^2), \tag{5}$$

where ω is the driving laser frequency and a is a constant close to unity, $a < 1$. In [7] it was found that for the Rydberg state under consideration, the Stark shift is approximately $0.7U_p$ where U_p is the ponderomotive energy.

From equations (3) and (4) we have

$$d_{\rm eff} = \frac{\sqrt{a\omega_{10}}}{2\omega}. \tag{6}$$

The generalization for the two-color field is straightforward. Note, however, that as $d_{\rm eff}$ depends on the field frequency, the interaction with the two fields $E_1(t)$ and $E_2(t)$ with frequencies ω_1 and ω_2 should be written as $d_{\rm eff}(\omega_1)E_1 + d_{\rm eff}(\omega_2)E_2$.

The effective dipole moment given by equation (6) for 400 nm laser wavelength is 2.94 a.u. This is about an order of magnitude higher than the dipole matrix elements of the transitions from ground to Rydberg states in argon [27]. This is an important difference with the previously suggested approaches [13, 16, 25, 28] where d is the dipole moment matrix element. As we will see below, this leads to the pronounced nonlinearity of the response for laser intensities around 10^{13} W cm^{-2}, while more than an order of magnitude higher intensities where considered in [28] to describe harmonic generation at the 5 photon resonance between 1s and 2p states of hydrogen.

The assumption of the quasi-free oscillations of the Rydberg states in the field is applicable when the amplitude of the oscillations is much less than the spatial extent of the electronic wave function in this state. This is the case for the used fields' parameters.

Note that making assumption (4) is in some sense similar to the approach used in the Keldysh theory where the transition probability is calculated using not the field-free upper state (i.e. the plane wave), but the state in which the interaction with the laser field is taken into account (the Volkov state) [29]. Here we also use the upper state (the Rydberg state) taking into account the modification of its energy by the laser field due to the Stark shift.

3.3. Discussion of the TDSE and the two-level model applicability

Several Rydberg levels could contribute to the experimental signal. This feature should be reproduced by the TDSE solution because the Rydberg states are well-described within this approach, while two-level model has only one excited state. Moreover, neither the one-electron TDSE, nor the two-level model reproduces the interference between the two channels of harmonic generation (via s–p and d–p transitions).

The observed bandwidth of the xFID line is much larger than the inverse radiation life-time of the excited level because of the limited resolution of the XUV spectrometer (about 60 meV at 15 eV). Opposite to this, within the TDSE approach this bandwidth is zero because this approach does not describe the spontaneous processes. The number of quantum approaches beyond the semi-classical approximation are developed recently [30, 31] to describe such type of phenomena. In the calculations presented below we consider the TDSE numerical solution at the limited time interval (0.5 ps), thus rendering very roughly the limited emission times. The two-level model allows more accurate (although semi-phenomenological) description of the limited lifetimes. Namely, the decay time of the excited state T_1 (longitudinal decay time) and the decay time of the dipole moment (or decay time of the coherence, transverse decay time) T_2 can be introduced in the Bloch equations. Time T_1 for the considered levels should be of the order of picoseconds or nanoseconds. In our calculations we set $T_1 = 10$ ps and checked that longer T_1 does not anyhow change the results. In [7] the transverse decay time for the Rydberg states was studied monitoring the retrieval of the xFID signal with the delay and T_2 from 6 ps to 30 ps were found. In the calculation we set $T_2 = 3$ ps. We use the value comparable with the experimental result but shorter to avoid very long (i.e. heavy) calculations.

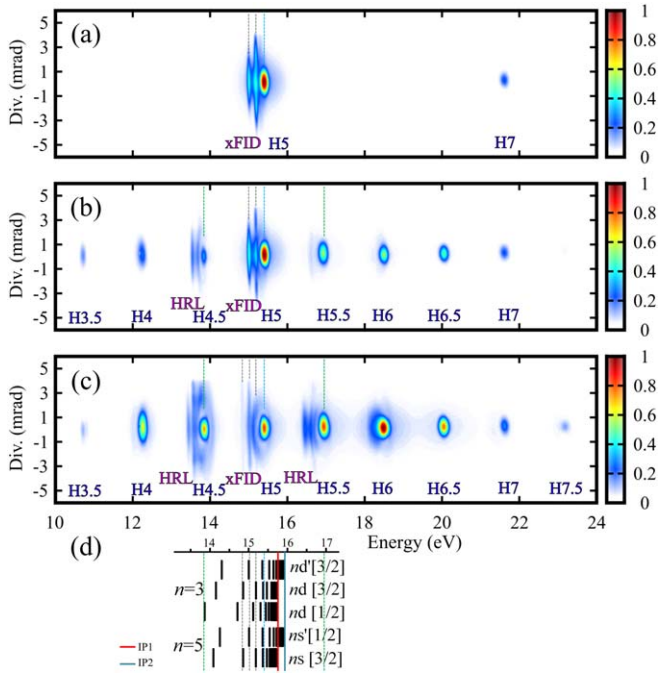

Figure 3. Experimental simultaneous observation of hyper-Raman Lines (HRL) and High-order Harmonics in argon, using two-color laser pulses. In (a), a spatio-spectrally resolved spectrum of light emitted by argon driven by 400 nm pulses. In (b), same as in (a) but the argon atoms are driven by a two-color (400 nm + 800 nm) field, where the intensity of the 800 nm is 0.9×10^{12} W cm^{-2}. The two pulses overlap in time. In (c), same as (b) but the intensity of the infrared was increased to 2.25×10^{12} W cm^{-2}. Harmonics orders are denoted according to the 400 nm energy. (d) Energy levels of argon in the corresponding range. Dashed lines correspond to the features shown on the upper panels.

The numerical solution for the two-level model is not very cumbersome, so we will use it to study the spatial properties of the generated fields (this study requires calculation of the atomic response in numerous spatial points). Opposite to this, the 3D TDSE numerical solution is heavy because we have to describe correctly Rydberg states which are large.

4. Results

4.1. Spatial structure

The spectrum emitted when argon atoms are driven using moderately strong ($\sim 10^{13}$ W cm^{-2}) 400 nm pulses is shown in figure 3(a). The well-collimated emission around 15.5 eV and 21.7 eV are respectively H5 and H7 (harmonic 5 and 7 of the 400 nm driving field). In addition to this conventional HHG emission, one can clearly notice the signature of XUV-Free Induction Decay (xFID) on the red-wing of H5. Indeed, more divergent narrow bandwidth spectral features at the field-free energies of Rydberg states are also present and are associated with xFID emission [7]. This xFID emission is a smoking-gun signature of the presence of a coherent superposition of electronic states. In this case, the electronic wavepacket is composed of a coherent superposition of the ground and few Rydberg states, identified respectively as 6s[3/2] and 4d[3/2] at 14.8 eV, 6s′[1/2] and 4d′[3/2] at 15.0 eV and 7s[3/2] and 5d[3/2] at 15.2 eV (see figure 3(d)).

In our experimental scheme, we first optimized the 400 nm pulse parameter to maximize the xFID emission at the field-free energies of the Rydberg states. Because these states are accessible through a resonant 5 photons transition, the intensity needed to induce xFID is below the one to efficiently generate non-resonant HHG. Indeed, figure 3(a) shows that the spectrum is dominated by H5 and xFID signals when the 400 nm pulse is alone. Because an experimental observable allows to directly monitor the efficiency with which the coherence between ground and Rydberg states is reached (xFID), it is straightforward to find the optimized experimental conditions that prepare the system in the required superposition of states.

Next we superimposed a 800 nm pulse that spatially and temporally overlaps with the 400 nm pulse. The spectrum of the XUV light emitted by argon, when driven by the two-color field is shown in figure 3(b). Note that the 800 nm field alone is not intense enough to generate HHG. One can first notice the presence of even, odd and half-integer harmonics (with respect to the 400 nm photon energy). In this case, the generation of even harmonics is allowed since the superposition of the 400 and the 800 nm fields is breaking the up-down symmetry of the interaction (or the half-cycle periodicity of the HHG process). In addition to even and odd

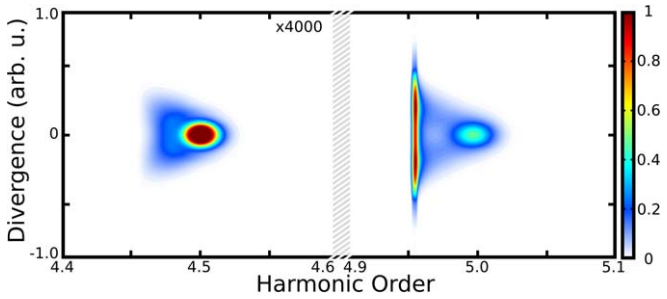

Figure 4. Spatially resolved XUV spectra near H4.5 (with respect to 400 nm) and H5 calculated using the two-level model atom driven by a two-color field (see text for more details). One can see both harmonics and their low-frequency satellites, corresponding to HRL (in the case of H4.5) and xFID (in the case of H5). The hyper-Raman Lines (HRL) is more divergent than the non-resonant HHG.

harmonics, we observe the presence of the HRL on the red-wings of harmonics adjacent to H5 (H4.5 and H5.5). The contribution of these HRL on the red-wings of harmonics gets even stronger when the IR intensity is further increased (see figure 3(c)). Note that the spectral positions of these HRL do not correspond in energy to any field-free atomic transitions and are located at $\pm\hbar\omega_{800}$ from the xFID emission ($\Omega_{\mathrm{xFID}} = (E_2 - E_1)/\hbar$). The fact that we observed clear HRL indicates that the IR induced Stark-shift is not sufficient to spectrally wash-out their signature.

In figure 3(c) we can see the curved spatio-spectral features near harmonic lines H4.5, H5 and H5.5. These features are similar to the ones provided by the long electronic trajectories contribution to the HHG in intense laser fields [32, 33]. The features in figure 3 cannot be directly attributed to these trajectories because the rescattering picture is inapplicable, even qualitatively, for the relatively low intensities used in our experiments. However, similar features should appear as soon as the harmonic response has a contribution whose phase depends on the laser intensity. Such dependence is typical for non-perturbative microscopic response [34] (and not only for the rescattering picture). The non-perturbative behavior is expectable for the considered resonance-induced phenomena under used laser intensities (which are much higher than typically used in conventional nonlinear optics, although lower than ones used for HHG).

We have calculated the spatially resolved far-field XUV spectrum emitted by a two-level model atom in the two-color field. We assume that (i) the generating beams are Gaussian with the same size, (ii) the thickness of the generating medium in the propagation direction is negligible (which is reasonable considering the effusive gas jet used in the experiment is thin), (iii) the medium position coincides with the beam focus. For the fields' intensities used in our experiments the resonant (H5) harmonic intensity calculated with the two-level model exceeds the intensities of H4.5 and H5.5 by orders of magnitude, in contradiction with the experimental result. This feature can be attributed to the weak non-resonant nonlinearity of the two-level system as following. Emission of the H4.5 and H5.5 from the coherently-populated upper state involves one 800 nm photon and one 400 mn photon thus it is due to the third order nonlinearity. This non-resonant nonlinearity in the two-level system is much weaker than in real atom, leading to the mentioned disagreement. However, the spectrum of every line separately is reasonably reproduced, see figure 4. The parameters of the calculation are the following: the transition frequency is 15.36 eV (4.955 of the 400 nm photon energy), $d_{\mathrm{eff}} = 2.94$ a.u. for the 400 nm driving field and $d_{\mathrm{eff}} = 5.88$ a.u. for the 800 nm one. The 400 nm intensity is 1.2×10^{13} W cm^{-2} and the 800 nm intensity is 10^{12} W cm^{-2}. The 800 nm pulse comes 50 fs later than the 400 nm one. Both driving pulses are 75 fs long and have Lorentzian time envelope. Note that using Lorentzian pulse shape (but not Gaussian or sin^2) turns out to be crucial for reproducing the experimentally observed properties. This is because the wide wings of the Lorentzian pulse adequately reproduce the dressing by the strong laser field far from the pulse center, as it was discussed in [20]. The XUV signal presented in figure 4 is saturated at the level of half of the maximal intensity.

In figure 4 we see that both H4.5 and H5 have low-frequency satellites (respectively the HRL and xFID) whose divergence is higher than the ones of the harmonics, in agreement with the experiment. However, experimentally both satellites have comparable intensity and spectral width while this is not the case in the calculation for the xFID. This can be attributed to the limited resolution of the spectrometer. Experimentally, this arises by smoothing narrow, high amplitude into wide, lower amplitude.

To understand the physical origin of the difference in the spatial width of the harmonics, the HRL and the xFID we present in figure 5 the intensity and phase of the atomic response for the harmonics and the HRL and xFID lines. In all cases the intensity demonstrates non-monotonic dependence on the radius, i.e. on the driving intensity. The intensity of the atomic response for the harmonics and the satellites have maximum at $r \approx 0.3r_0$. This maximum can be explained as following: the dependence of the driving intensity on r leads to the dependence of the Stark shift of the upper state on r; the maximum originates from the exact multi-photon

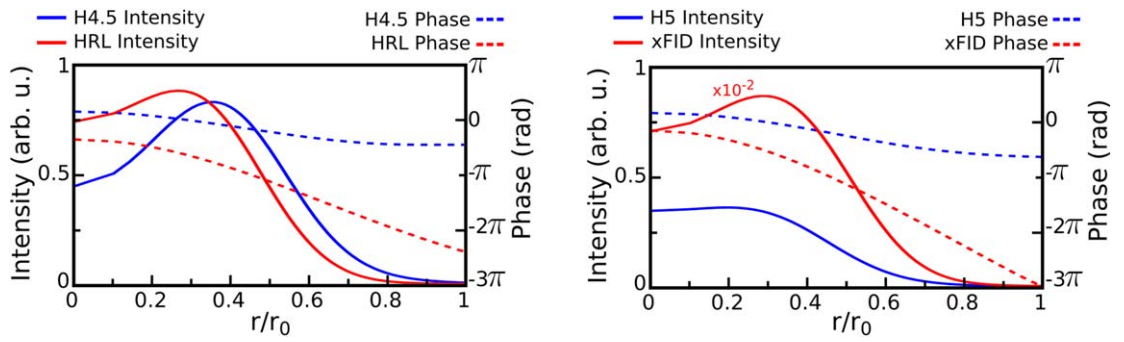

Figure 5. Intensity (solid line) and phase (dashed line) of the atomic response as a function of a distance from the axis. Calculation via two-level model for the exact H4.5, H5 harmonics (blue lines) and their low-frequency satellites corresponding to HRL and xFID (red lines). r_0 is the driving beam size (at the e^{-1} intensity level), other parameters are the same as in figure 4.

resonance with the Stark-shifted level. Although specific position of this maximum depends on the used parameters of the calculation (peak laser intensity, etc), in general the non-monotonous behavior of the response due to intensity-dependent detuning from the resonance is rather general. Note that laser intensity-dependent ponderomotive shift of states leads to resonant features in the photoelectronic spectrum of above-threshold ionization known as Freeman resonances [35].

One can see that both intensity and phase behave remarkably similarly for the HRL (left panel) and xFID (right panel). This is a strong evidence that the generation of both satellites (HRL and xFID) have the same origin.

The phases of the harmonics and the ones of the satellites behave differently. Namely the harmonic demonstrates total phase variation close π when the Stark-shifted level passes the multiphoton resonance. The satellites' phase is more sensitive to the driving intensity, the total phase variation is close to 2π. One can suppose that this is because the satellite phase is controlled by the phase of the upper state which is accumulated during the whole driving pulse(s), so small change in the detuning (due to the Stark-shift dependence on the intensity) leads to pronounced change in the phase. The pronounced dependence of the response phase leads to the wide angular distribution of the satellite in the far-field shown in figure 4.

In order to gain more insight about the build-up of the emission features, we will experimentally and theoretically investigate the influence of the IR pulse intensity and of the 400–800 nm delay on the HRL generation.

4.2. IR intensity scan

Figure 6(a) shows the spatially-integrated spectrum near the ionization threshold as a function of the IR intensity. Figure 6(c) shows the corresponding differential signal, where the signal induced by the 400 nm pulse alone (the undressed emission) is subtracted for each intensity, so that within this differential spectrum negative (blue) signal comes from IR-induced depletion and that the red (positive) signal comes from emission induced by the presence of the IR field.

As the IR intensity increases, the xFID and the H5 emission (between 15 and 15.5 eV) get depleted while the H4.5, H5.5 and their HRL satellite (around 13.5–14 eV and 16.4–17 eV respectively) get stronger. One can also see an asymmetric behavior below- and above-threshold. Indeed, for IR intensity below 1.3×10^{12} W cm^{-2}, the above-threshold emission is dominated by H5.5 while the below-threshold emission is made of equal contribution between H4.5 and its HRL satellites. This asymmetry is well reproduced by the 3D-TDSE calculations, which are presented in figures 6(b) and (d). Note that the TDSE calculations presented do not aim at exactly matching the experiment, especially the exact resonant levels profile, which is very sensitive to the potential used, or the exact cross sections. The goal was to grasp the principle of the dressing effect of the field, one photon energy above and below, which is nicely reproduced here. One can see in both experimental results and theoretical calculation that within this intensity range, the HRL are very stable against IR intensity. The 400 nm electric field creates a coherent superposition of states while the required IR field to drive HHG from the laser-dressed system remains weak and allows the observation of both HHG and HRL.

4.3. Delay scan

Because we used two-color field, the relative delay between the 400 and 800 nm is also an other parameter that we scan to gain information about the interplay between HHG and HRL. The experimental data are presented in figure 7(a). The negative time delays mean that the IR pulse comes before the 400 nm pulse. At large negative delays, we observe delay-independent xFID emission around 15 eV. This means that the IR is too weak to excite

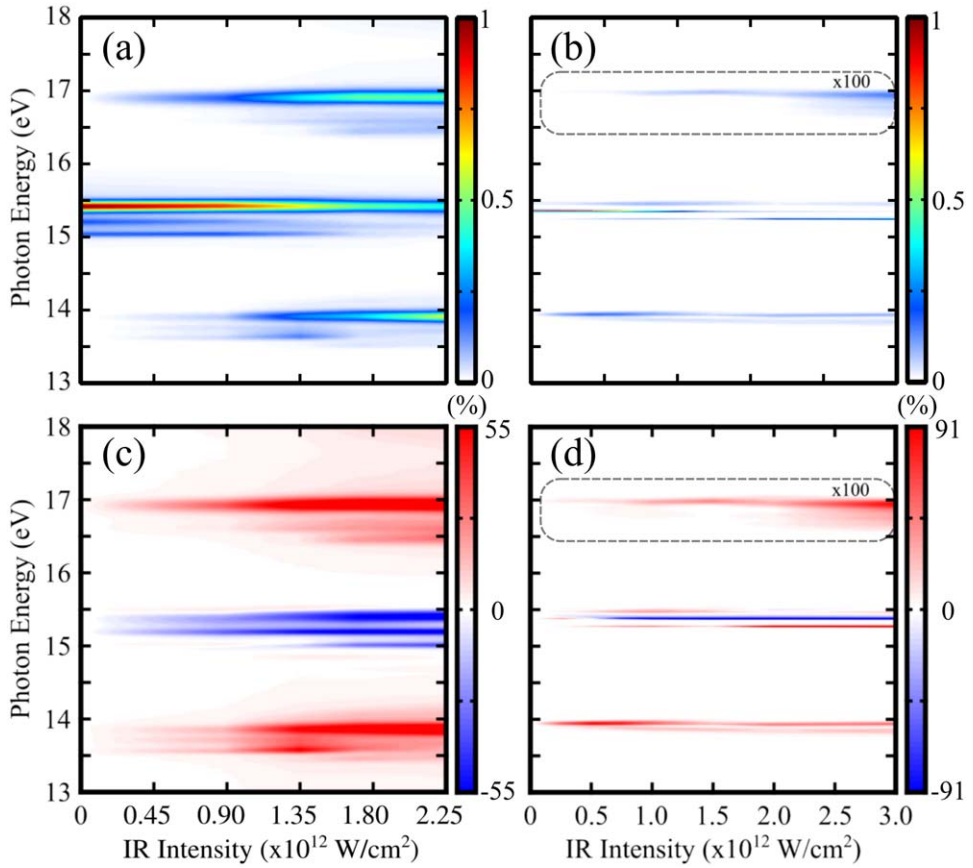

Figure 6. Scaling of the emission with the increase of the IR intensity near the ionization threshold. (a) Experimentally measured spatially integrated near-threshold XUV spectrum as a function of the IR laser intensity. The 400 nm pulse parameter are kept constant, and the time-delay between the two pulses is zero. (b) 3D-TDSE calculation of the near-threshold XUV emission as a function of the IR intensity. The IR intensity is scanned from 0 to 3×10^{12} W cm^{-2} and the 400 nm intensity was kept constant (10^{13} W cm^{-2}). The duration of both pulses were set to be 75 fs FWHM in the calculation. (c) and (d) Differential signal of (a) and (b), with respect to the undressed (400 nm only) spectrum, in percent of the maximum undressed emission.

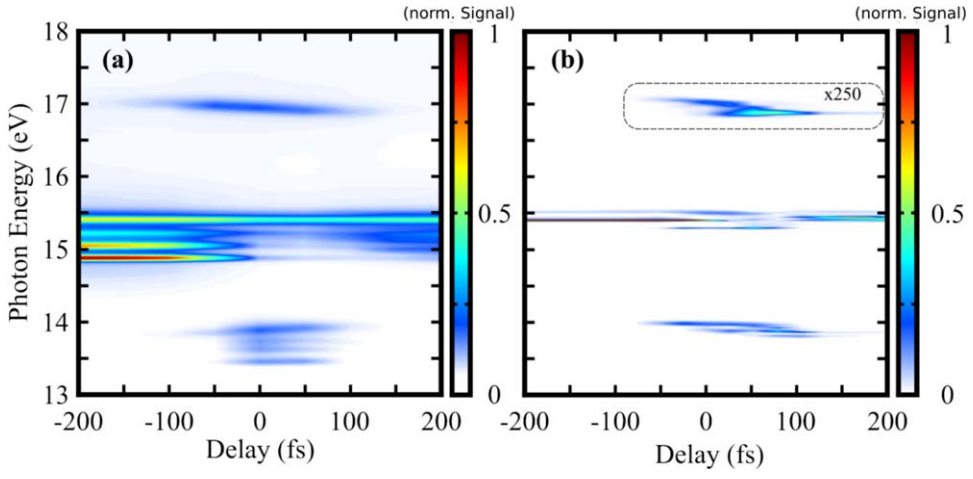

Figure 7. Time-resolved near-threshold emission spectrum as a function of the delay between the 400 and the 800 nm pulses. (a) Experimentally measured time-resolved near-threshold XUV spectrum as a function of 400–800 nm delay. The IR intensity is set to ~0.45×10^{12} W cm^{-2}. (b) 3D-TDSE calculation of the time-resolved near-threshold XUV emission. The IR intensity is 3×10^{12} W cm^{-2} and the 400 nm intensity is (10^{13} W cm^{-2}). The duration of both pulses were set to be 75 fs FWHM in the calculation.

the system alone. Around zero delay, one sees above-threshold features corresponding to H5.5. The fact that no HRL is observed on the red-wings of H5.5 at this intensity is due to the asymmetry of below- and above-threshold emission, visible in the IR intensity scan (see figures 6(a) and (c)) but not well understood yet.

Table 1. Central energy, experimentally measured energy slope with respect to the 400 nm pulse–800 nm pulse delay and the photon combination associated with it for each harmonic sideband between H3.5 and H6.5. A ~0.6 eV ps^{-1} chirp has been imposed to the 800 nm pulse.

Line	Central energy (eV)	Energy slope with delay (eV ps^{-1})	Photon combination
H6.5	20.1	0.60	$5 \times 400\ nm + 400\ nm + 800\ nm$
H6	18.6	1.3	$5 \times 400\ nm + 2 \times 800\ nm$
H5.5	17.0	−0.60	$5 \times 400\ nm + 400\ nm - 800\ nm$
H5	15.5	0	$5 \times 400\ nm$
H4.5	13.9	0.53	$5 \times 400\ nm - 400\ nm + 800\ nm$
H4	12.4	−1.3	$5 \times 400\ nm - 2 \times 800\ nm$
H3.5	10.8	−0.63	$5 \times 400\ nm - 400\ nm - 800\ nm$

Below-threshold, we observe the presence of H4.5 and HRL satellites around time zero. One can see that the HRL emission is delayed by ~20 fs after the center of the cross-correlation. This is due to the fact that the HRL lines are generated solely after the creation of a coherent superposition of states, which occurs at the peak intensity of the 400 nm pulses. After the temporal overlap between the 800 and 400 nm pulses, the only spectral features that last are the xFID and H5 emission. This means that both fields are necessary to observe significant HRL emission. In the theoretical calculation presented in figure 7(b) we also see that HRL, both below- and above-threshold are generated mainly within the cross-correlation.

As the ground state of the atomic system is spherically symmetric, the total number of photons being absorbed by the system must be odd in order to reach a state which is allowed to emit dipole radiation when being in a coherent superposition with the ground state. In our experiment, the xFID observed around 15 eV is coming from a coherent superposition between the p- ground state and *n*s-/*n*d- Rydberg states which have been created through 5 photons absorption. The HRL lying 1.55 eV below- and above- this xFID emission cannot be explained by a direct single IR emission/absorption from the Rydberg states, because it would imply that an even number of photons would have been absorbed ($5 \times 400\ nm \mp 1 \times 800\ nm$), preventing the emission of XUV. Indeed, the HRL lying 1.55 eV below- and above- the Rydberg states comes from the emission/absorption of one 400 nm combined with the absorption/emission of one 800 nm, from the Rydberg states ($5 \times 400\ nm \mp 1 \times 400\ nm \pm 1 \times 800\ nm$). This is why after the cross-correlation, when the 400 nm field is off, the 800 nm field itself does not generate HRL from the coherent superposition of states, which lives for picoseconds.

A slight positive chirp (lower energies first) has been imposed to the 800 nm pulse so that its central frequency get modulated by ~0.6 eV ps^{-1}. One can see that the energy of the harmonics' sidebands get tilted (H4.5 and H5.5 respectively around 14 eV and 17 eV on figure 7(a)). The slope of the energy of emission with respect to the delay has been extracted (see table 1). This unambiguously gives us the number of 800 nm photons involved in the 400 nm/800 nm photons combination leading to these sidebands. The tilt of the harmonics generated at a given energy below or above the threshold H5 have opposite signs. This means that these harmonics are triggered by the absorption of 5×400 nm photons, followed by absorption/emission of photons from the 400 nm and/or the IR field. Except for H4 and H6 that come from H5 $\pm 2\hbar\omega_{800}$, they all come from the combination of the 400 and 800 nm fields, verifying that total number of photon involved remains odd. Remarkably, the number of 400 and 800 nm photons involved appears to be equal for the HRL near H5.5 and H6.5 as well as near H4.5 and H3.5. However, as seen on figure 3(c), only HRL around H5.5 and H4.5 are clearly visible experimentally. This intriguing asymmetry could be the signature of different dynamics of excitation in the HRL process, and calls for additional experimental and theoretical investigations.

Note that interestingly, unlike the non-resonant features, the HRL do not appear tilted, indicating a fundamentally different mechanism induced by the resonances. From our studies using the two-level model we see that the HRL emission is temporally more confined near the peak of the IR pulse than the harmonic emission. This can be attributed to the fact that the Stark shift of the Rydberg state due to the IR field is comparable to the one due to the second harmonic field (the IR intensity is lower, but the shift is inverse proportional to the frequency squared, see equation (5)). Taking into account the Stark shift means considering higher-order multiphoton processes: HRL at the red side of H4.5 can be generated as $5 \times 400\ nm - 1 \times 400\ nm + 1 \times 800\ nm$ where 5×400 nm means the coherent excitation of the Rydberg state; if we would like to take into account the IR-field Stark-shifted Rydberg state we should denote it as $5 \times 400\ nm + 1 \times 800\ nm - 1 \times 800\ nm$. So the HRL emission could be partly attributed to processes involving more than one IR photon, leading to a temporal emission more confined near the peak of the IR pulse. Thus the frequency of this line is given by the IR frequency near the peak of the IR pulse, i.e. the central IR frequency, resulting in less tilt of the HRL in figure 7(a).

An additional possible source of temporal confinement of the resonant processes could be the chirp of the laser pulses. The instantaneous Stark shift of the resonant levels is modulated along the laser pulse envelope. To significantly excite these levels, the instantaneous photon frequency must match the instantaneous level position. In a chirped pulse, the photon frequencies arise at different moments in the pulse, such that the resonance condition can be confined to only a portion of the whole pulse duration.

5. Discussion and conclusions

The presence of HRL ($\Omega_{\mathrm{HRL}} = (E_2 - E_1)/\hbar + 2q'\omega_0$) together with high-order harmonics ($\Omega_{\mathrm{HHG}} = 2q\omega_0$) was predicted a long time ago by many theoretical calculations. The generation of HRL requires a system in a coherent superposition of states (characterized by their energy E_1 and E_2, for example). In order to be observable in an experiment, the spectral position of the HRL lines must be more or less constant as a function of time within the laser pulse. However, they have never been identified experimentally, probably because of temporal and spatial smearing of the lines resulting from the Stark-shift of the states in strong laser pulses.

Here, we partially decoupled the preparation of the coherent superposition of states and the HHG+HRL emission by using a two color laser field. The electronic wavepacket is prepared using a resonant few-photon transition (with a 400 nm pulse), from which a relatively weak low-frequency field (800 nm) is driving HHG and HRL. These processes are efficient when the two laser pulse are temporally overlapped. We have scanned the intensity of the 800 nm pulse and varied the delay between the 400 and 800 nm pulses in order to gain information about the different behavior of HRL and HHG.

The interest of HRL in terms of technological application, for example as a photon source, still remains uncertain since they are hard to observe experimentally. The light-driven spectrum is more than often dominated by HHG. However, for certain conditions the red-shifted satellites due to HRL could be a seeding for high-order parametric processes considered theoretically in [34]. As it was shown in this paper, for specific frequencies of the generated fields such processes are phase-matched, and the propagation leads to the exponential growth of the red-shifted satellites; the effective generation of the red-shifted satellites of high harmonics was observed in [36].

Moreover, the particular conditions where both HRL and HHG are present in the spectrum is fundamentally interesting to study. In the same fashion that High-Harmonic Spectroscopy provides high-resolution spatio-temporal informations about ground (valence) state electrons, HRL spectroscopy might provide high-resolution spatio-temporal information about excited (Rydberg) state electrons. The link between the far-field spatial profile of the HRL and the Freeman-type resonances can be the first step in this direction.

Acknowledgments

We thank R Taïeb for fruitful discussion and R Bouillaud and L Merzeau for technical assistance. We acknowledge financial support of the French National Research Agency (ANR), through ANR-MISFITS and IdEx Bordeaux LAPHIA (ANR-10-IDEX-03-02). This project has received funding from the European Research Council (ERC) under the European Unions Horizon 2020 research and innovation program no. 682978—EXCITERS. SB acknowledges the Vanier Scholarship. Theoretical studies were supported by the Russian Science Foundation (Grant No. 16-12-10279).

References

[1] Ferray M, L'Huillier A, Li X F, Lompre L A, Mainfray G and Manus G 1988 *J. Phys. B: At. Mol. Opt. Phys.* **21** L31
[2] McPherson A, Gibson G, Jara H, Johann U, Luk T S, McIntyre I A, Boyer K and Rhodes C K 1987 *J. Opt. Soc. Am.* B **4** 595–601
[3] Krausz F and Ivanov M 2009 *Rev. Mod. Phys.* **81** 163
[4] Lewenstein M, Balcou P, Ivanov M Y, L'Huillier A and Corkum P 1994 *Phys. Rev.* A **49** 2117
[5] Bengtsson S *et al* 2017 *Nat. Photon.* **11** 252–8
[6] Cao W, Warrick E R, Fidler A, Neumark D and Leone S R 2016 *Phys. Rev.* A **94** 053846
[7] Beaulieu S, Bloch E, Barreau L, Comby A, Descamps D, Géneaux R, Légaré F, Petit S and Mairesse Y 2017 *Phys. Rev.* A **95** 041401(R)
[8] Beaulieu S *et al* 2016 *Phys. Rev. Lett.* **117** 203001
[9] Yun H, Mun J H, Hwang S I, Park S B, Ivanov I A, Nam C H and Kim K T 2018 *Nat. Photon.* **12** 620–4
[10] Millack T and Maquet A 1993 *J. Mod. Opt.* **40** 2161
[11] Plaja L and Roso L 1993 *J. Mod. Opt.* **40** 793
[12] Gauthey F I, Keitel C H, Knight P L and Maquet A 1995 *Phys. Rev.* A **52** 525
[13] De Luca S and Fiordilino E 1996 *J. Phys. B: At. Mol. Opt. Phys.* **29** 3277
[14] Pons M L, Taieb R and Maquet A 1996 *Phys. Rev.* A **54** 3634
[15] Di Piazza A and Fiordilino E 2001 *Phys. Rev.* A **64** 013802
[16] Di Piazza A, Fiordilino E and Mittleman M H 2011 *Phys. Rev.* A **64** 013414
[17] Zhou Z Y and Yuan J M 2008 *Phys. Rev.* A **77** 063411

[18] Kelley A M 2010 *Annu. Rev. Phys. Chem.* **61** 41
[19] Ziegler L D 2006 Hyper-Raman spectroscopy *Handbook of Vibrational Spectroscopy* ed J M Chalmers and P R Griffiths (New York : Wiley)
[20] Fareed M A, Strelkov V V, Thiré N, Mondal S, Schmidt B E, Légaré F and Ozaki T 2017 *Nat. Commun.* **8** 16061
[21] Strelkov V V, Platonenko V T and Becker A 2005 *Phys. Rev.* A **71** 053808
[22] Strelkov V V, Sterjantov A, Shubin N and Platonenko V T 2006 *J. Phys. B: At. Mol. Opt. Phys.* **39** 577
[23] Muller H G 1999 *Phys. Rev.* A **60** 1341
[24] Allen L and Eberly J H 1987 *Optical Resonance and Two-level Atoms* (New York: Dover)
[25] Fiordilino E 1999 *Phys. Rev.* A **59** 876
[26] Bloch F and Siegert A 1940 *Phys. Rev.* **57** 522
[27] Zatsarinny O and Bartschat K 2006 *J. Phys. B: At. Mol. Opt. Phys.* **39** 2145
[28] Fiordilino E, Morales F, Castiglia G, Corso P P, Daniele R and Strelkov V V 2017 *J. Opt. Soc. Am.* B **34** 2673
[29] Keldysh L V 1965 *Sov. Phys. JETP* **20** 1307
[30] Bogatskaya A V, Volkova E A, Kharin V Y and Popov A M 2016 *Laser Phys. Lett.* **13** 045301
[31] Magunov A I and Strelkov V V 2017 *Phys. Wave Phenom.* **25** 24
[32] Merdji H, Kovačev M, Boutu W, Salières P, Vernay F and Carré B 2006 *Phys. Rev.* A **74** 043804
[33] Catoire F *et al* 2016 *Phys. Rev.* A **94** 063401
[34] Strelkov V V 2016 *Phys. Rev.* A **93** 053812
[35] Freeman R R, Bucksbaum P H, Milchberg H, Darack S, Schumacher D and Geusic M E 1987 *Phys. Rev. Lett.* **59** 1092
[36] Hort O, Dubrouil A, Descamps D, Petit S, Burgy F, Mével E, Constant E and Strelkov V *Nat. Phys.* submitted